Core/Shell Particles Containing Liquid Cores: Morphology Prediction, Synthesis, and Characterization

André J. P. van Zyl,[†] Ronald D. Sanderson,[†] Deon de Wet-Roos,[†] and Bert Klumperman*[,†,‡]

Dutch Polymer Institute, Division of Polymer Science, Department of Chemistry, University of Stellenbosch, Private Bag X1, Matieland 7602, South Africa, and Laboratory of Polymer Chemistry, Eindhoven University of Technology, P.O. Box 513, 5600 MB Eindhoven, The Netherlands

Received May 9, 2003; Revised Manuscript Received August 25, 2003

ABSTRACT: The ability to synthesize core/shell particles with distinct geometries is becoming increasingly important due to their potential applications. In this study structured particles with liquid cores and polymeric shells were synthesized by an in situ miniemulsion polymerization reaction. The resulting materials were used to evaluate morphology prediction models based on thermodynamic considerations. Results showed that thermodynamic models are inadequate for the morphology prediction of in situ polymerized species. For particles prepared in this way, kinetic influences, e.g. anchoring effects, chain mobility, and viscosity, play a significant role in defining the end morphology of the particles.

Introduction

Core/shell particles have received considerable attention over the past decades.[1,2] Because of the distinct geometry of core/shell particles, numerous applications have evolved which include impact modifiers and toughening agents. As a result of the versatility of the core/shell morphology concept, different core materials are being investigated, leading to terminology such as microcapsules, encapsulation, container particles, and even voided particles. Hollow or void filled particles can serve as synthetic pigments to contribute to the opacity of coatings through light scattering or as gloss enhancers for paper coatings.[3] When filled with a liquid, these microcapsules can be used as controlled and sustained drug delivery systems in the pharmaceutical industry,[4,5] to prevent encapsulated volatile compounds from evaporation or susceptible compounds from oxidative decomposition and for safe handling of toxic substances.

Core/shell particles can be prepared via various routes of which a two-stage seeded emulsion polymerization was the first general method developed to prepare latex particles featuring this unique structure.[6] In this instance the second stage monomer is polymerized in the presence of the core seed latex which can either be prepared beforehand in a separate step (so-called "dead" or inactive seeding) or in situ during the emulsion polymerization (so-called "live" or active seeding). Other methods soon followed such as suspension cross-linking,[7] coacervation,[8] interfacial polymerization,[9] solvent evaporation,[10] and vesicle template polymerization.[11]

The synthetic route for the preparation of core/shell particles with liquid cores is slightly different from the conventional emulsion polymerization systems because of the high hydrophobicity and low water solubility of the core oil. In conventional emulsions no transport of the core liquid into micelles will take place. This ultimately results in an oily layer being present at the end of the reaction. Miniemulsion polymerizations, however, have proved to be a suitable method for the preparation of these types of systems.[12] By subjecting the oil/water/surfactant/cosurfactant system to high shear, the oil, which consists of the core liquid and monomer, will form droplets from which particles will develop during polymerization. In addition, phase separation can take place upon polymerization with consequent formation of particles with the required morphology. High shear fields can be created by devices such as ultrasonicators, homogenizers, and microfluidizers.

Depending on the polymerization parameters and conditions, the reaction can yield particles with various morphologies ranging from core/shells, via acorn or hemispheres, to heteroaggregates or inverted core/shells. These morphologies can be characterized through well-established characterization techniques such as TEM, SEM, or AFM[13] and also via less well-known ones, e.g., solid-state NMR,[14] SAXS,[15] and dielectric analysis.[16]

The ability to predict three-phase interactions in shear and electrical fields was introduced in 1970 by Torza and Mason, who studied two immiscible hydrocarbons in water.[17] Since then, numerous researchers have successfully applied this method to predict particle morphologies by expanding this concept to polymer/hydrocarbon particles[18] as well as polymer/polymer particles.[19] However, this model does not always hold for emulsion polymerization systems, as shown by Sundberg et al.[20−23] This is a result of the typical components, e.g., surfactant, initiator, chain transfer agents, and monomer present in the system, which may cause deviation from the thermodynamic equilibrium.

In this paper core/shell latexes based on poly(butyl acrylate) (PBA) as shell, and hexadecane (HD) as core liquid, are studied. Different combinations of low-viscosity core liquids and polymer were evaluated in terms of surface and interfacial tensions, followed by morphology predictions for the different permutations. The core oils were selected on the basis of their different hydrophobicities. PMMA was chosen to act as a second (glassy) shell around the initial rubbery shell to increase the particle strength and stability during analysis. The

[†] University of Stellenbosch.
[‡] Eindhoven University of Technology.
* Corresponding author.

10.1021/ma034596x CCC: $25.00
Published on Web 10/14/2003

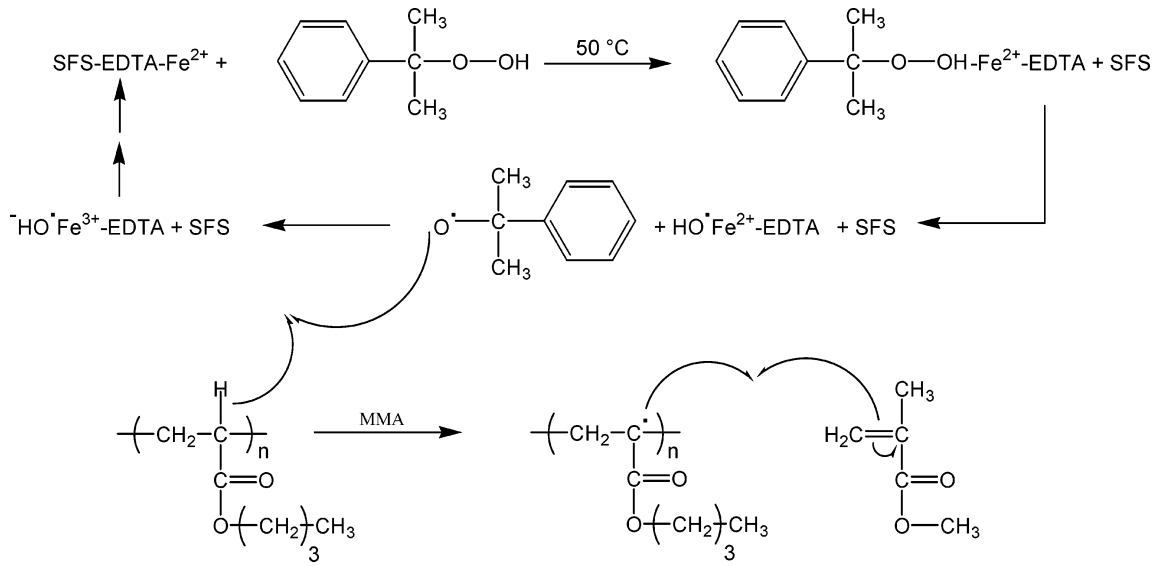

Figure 1. Schematic representation of the grafting reaction between MMA and PBA in the presence of an interfacial redox initiator system.

particles were synthesized using a miniemulsion polymerization process followed by a redox-grafting polymerization step to accomplish the secondary shell formation.

Experimental Section

Materials. Butyl acrylate (BA, 99.5%) (Hoechst) and methyl methacrylate (MMA, 99.9%) (ICI Chemicals and Polymers) were washed with a 0.3 M potassium hydroxide (KOH, 85%) (Associated Chemical Enterprises) solution, followed by distillation at reduced pressure to remove the inhibitor. Monomers were stored at −12 °C prior to use. Sodium dodecyl sulfate (SDS, 90%) (BDH); potassium persulfate (KPS, 99+%), sodium metabisulfite (SMBS, 97%), iron(II) sulfate ($FeSO_4$, 99+%), ethylene glycol dimethacrylate (EGDMA, 98%), cumyl hydroperoxide (CHP, 80%), sodium formaldehyde sulfoxylate (SFS) (all Aldrich); toluene (99.9%) (Riedel-de Haën); ethylenediaminetetraacetic acid, disodium salt (EDTA, 99%), methanol (MeOH, 99.8%) (both ACROS); and sodium bicarbonate (99.5%) (Saarchem) were used as received. Distilled deionized water, obtained from a Millipore Milli-Q purification system, was used. Hexadecane (HD, 99%), decane (D, 99+%), 1-octanol (O, 98%) (all ACROS), paraffin oil (PO), olive oil (OO, highly refined) (both from Aldrich), and silicon oil (SO) (SA Silicones) were employed as possible core oils. 1,1′-Azobis(cyclohexanecarbonitrile) (98%) (Aldrich) was used as received, and 2,2′-azobis(isobutyronitrile) (AIBN, 98%) (Delta Scientific) was recrystallized from methanol.

Polymerization of BA for Surface Tension Experiments. PBA was synthesized by free-radical solution polymerization in order to ensure a surfactant-free polymer, which would otherwise have a significant influence on surface tension evaluations due to surfactant interaction. Toluene (269 g) and monomer (89 g, 6.94×10^{-1} mol) were added into a 500 mL round-bottom flask which was immersed in a heated oil bath. The flask was equipped with a reflux condenser and nitrogen feed. The initiator 1,1′-azobis(cyclohexanecarbonitrile) (0.45 g (1.84×10^{-3} mol) in 2 g of toluene) was added, and the reaction was allowed to continue for 21 h at 70 °C. The molar mass (M_w) of the synthesized PBA was 94 561 g/mol ($M_w/M_n = 2.76$) relative to narrow PMMA standards.

Latex Synthesis. PBA/HD core/shell particles were synthesized by a miniemulsion polymerization reaction (formulation shown in Table 1). Butyl acrylate, hexadecane, and sodium bicarbonate were premixed with a SDS/water solution for 1 h, after which a miniemulsion was obtained by sonicating the mixture with a Sonics & Materials Inc. Vibracell VCX 750 ultrasonicator for 30 min at 90% amplitude (161.69 kJ). During this period the solution was continuously stirred in a jacketed vessel to avoid polymerization due to heating. After miniemulsification the solution was transferred to a 250 mL glass reactor, suspended in a thermostated oil bath and equipped with a condenser and nitrogen purge. Polymerization was achieved by adding KPS initiator and SMBS at 80 °C. Continuous purging was performed by bubbling nitrogen through the latex solution. EGDMA (30 wt % to monomer) was added 45 min after the start of the reaction to give more stability to the rubbery shell through cross-linking. The reaction was allowed to continue for 3.5 h, after which it was cooled to 50 °C.

Table 1. Typical Formulation for a PBA/HD Core/Shell Polymerization

	(g)	(mmol)
kettle charge		
SDS	0.7	2.427
DDI	70	
BA	3.85	30.038
hexadecane	3.01	13.292
sodium bicarbonate	0.204	2.428
initiator solution		
KPS	0.0247	0.091
SMBS	0.0174	0.092
purge gas		
N_2		
cross-linker		
EGDMA	1.16	5.852
graft reaction		
MMA	3.85	38.454
CHP	0.25	1.643
$FeSO_4 \cdot 7H_2O$	0.0104	0.037
EDTA	0.4	1.075
SFS	0.4	2.595

To add a second shell, a redox initiator system consisting of cumyl hydroperoxide/Fe^{2+}/ethylenediaminetetraacetic acid/sodium formaldehyde sulfoxylate (CHP−Fe^{2+}−EDTA−SFS) was used in the grafting of MMA onto the PBA shell.

EDTA was used as chelating agent and SFS as reducing agent[24,25] to reduce Fe^{3+} to Fe^{2+} during the redox polymerization. A schematic representation of the reaction can be seen in Figure 1.

Interfacial and Surface Tension Measurements and Consequent Spreading Coefficient Calculations. To be able to predict morphology, it is necessary to preevaluate the surface properties of the polymer, oils, and surfactant/cosurfactant in question. This was done by using a torsion balance and a platinum Du Noüy ring for surface tension evaluations of the different oils and for interfacial tension measurements

of the oil/water combinations. Interactions between the polymer and oils, as well as polymer/water interactions, were evaluated by using a Cahn DCA contact angle analyzer. For contact angle evaluations polymer samples were prepared by dip-coating nylon strings into a polymer solution and allowing them to dry in a dust-free environment before analysis. The contact angle could be calculated from force/immersion depth curves by using the modified Young's equation[26]

$$\theta = \cos^{-1}\left(\frac{F}{p\gamma}\right) \tag{1}$$

where F is the force at zero immersion depth, p is the perimeter of the sample, and γ is the surface tension of the oil. For the oil/polymer and polymer/water combinations, Young's equation[27]

$$\gamma_{sl} = \gamma_{sv} - \gamma_l \cos\theta \tag{2}$$

was used where γ_{sl} is the solid/liquid interfacial tension, γ_{sv} is the solid/vapor interfacial tensions, γ_l is the surface tension of the liquid, and θ is obtained from eq 1. The value of γ_{sv} can be obtained from literature or can be calculated.[27,28] Oil/water interfacial tensions and surface tensions of the different liquids (γ_l) were directly obtained with the torsion balance. However, values from literature could also be used.[29] The Du Noüy ring was cleaned in concentrated H_2SO_4 and rinsed with distilled water and acetone before use and also in between consecutive measurements for accuracy. For all of the above measurements at least three readings were taken, and the mean value was used in further calculations.

As temperature is an important parameter in surface properties of polymers and oils,[30] the temperature was regulated to be 20.5 ± 1 °C and the humidity was kept constant by conducting experiments in a controlled environment laboratory.

Analytical Techniques. *Atomic Force Microscopy (AFM).* One droplet of an undiluted latex solution was deposited on an angularly placed, flat silica surface so that the polymer formed a smooth film consisting of a few monolayers of latex particles. Excess water was removed by blotting with filter paper. AFM experiments were carried out using a Topometrix Explorer with silicon noncontact tips from Nanosensors GmbH (Germany). AFM images were obtained at ambient conditions while operating the instrument in noncontact mode.

Transmission Electron Microscopy (TEM). Samples for TEM measurements were prepared following a procedure of Sue et al.,[31] who proposed a novel staining technique for studying saturated polyacrylate rubbers. Sample preparation was done by precipitating and drying the latex to obtain a fine powder. The powder was subsequently embedded in Spurr's resin and cured at 60 °C for 16 h. The epoxy resin block was then placed in styrene for 1 h, after which it was washed with water and patted dry. The block was transferred to a glass jar containing 0.5 g of OsO_4 and left there for 3 days to allow adequate staining by the vapor. To complete the process, the block was left in a fumehood for 24 h to allow excess OsO_4 to evaporate, after which it was microtomed at ambient temperature with a Reichart Ultracut S (Leica, Vienna, Austria) ultramicrotome, with a diamond knife, to produce slices with a thickness of 100 nm. These slices were placed on a copper grid. Analyses were done on a JEM-200CX (JEOL Ltd., Tokyo, Japan) TEM.

A nondestructive TEM sample preparation procedure was also followed. For this procedure 2 mL of the latex was added to an excess of MeOH to aid precipitation of the particles. The particles were redispersed by shaking and transferred to a copper TEM grid by pipet. The grid was left to dry at ambient temperature before analyses were performed. No staining was applied to the dried particles. Contrast between the core and shell was the result of the combined effects of the different path lengths and densities of the constituting materials. This resulted in increased scattering of the incident e^- beam from the wall material, resulting in a darker region on the TEM images. Analyses were done on a JEM-200CX and 2000FX (JEOL Ltd., Tokyo, Japan) TEM. The copper grids were prepared by the deposition of a thin film of carbon for increased strength and conductivity of the film.

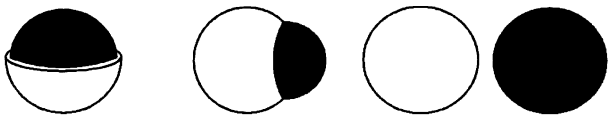

Complete engulfment $S_1<0, S_2<0, S_3>0$ | Partial engulfment $S_1<0, S_2<0, S_3<0$ | No engulfment $S_1<0, S_2>0, S_3<0$

Figure 2. Schematic representation of different morphological configurations with the assigned spreading coefficients. The two immiscible phases (shown here as black and white drops) are designated as phase 1 and 3. The continuous medium is phase 2.

Results and Discussion

Morphology predictions were conducted using the methods of Torza and Mason[17] as well as of Waters.[32,33] Predictions according to Torza and Mason were done by experimental examination of the interfacial tension between the three phases (oil/water, oil/polymer, and polymer/water) of the system. This in turn allowed the calculation of the spreading coefficients of a specific oil/polymer system which makes it possible to predict the morphology, i.e., core/shell or acorn, of the formed particles. The spreading coefficient is defined as

$$S_i = \gamma_{jk} - (\gamma_{ij} + \gamma_{ik}) \tag{3}$$

where γ is the interfacial tension (i, j, and k refer to the three phases) and designating phase 1 to be that for which $\gamma_{12} > \gamma_{23}$ so that $S_1 < 0$. Complete engulfing (core/shell) occurs if $S_3 > 0$ and $S_2 < 0$. On the other hand, partial engulfing (acorn shape) will be preferred when $S_2 < 0$ and $S_3 < 0$. A schematic view of the different configurations with the assigned spreading coefficients can be seen in Figure 2. In calculation of the spreading coefficients for the investigated system, the continuous phase (water, w) was taken as phase 2, the polymer phase (p) was assigned to phase 1, and the oil phase (o) was assigned to phase 3. The reason for this assignment is that it fulfills the requirement $\gamma_{12} > \gamma_{23}$.

The value for the γ_{sv} of PBA was obtained from literature and was taken as 33.7 mN m^{-1}.[27] Values for the contact angles between the oil and polymer (θ_{op}) and between the polymer and water (θ_{pw}) as well as the calculated interfacial tensions and spreading coefficients can be seen in Table 2.

The influence of hexadecane as costabilizer on the oil/water and oil/polymer interface was also investigated (Table 2). This was done to confirm work done by Landfester et al.,[34] who reported that hexadecane does not act as a surface active agent. The hydrophobe will act as a "superswelling" agent whereas a fatty alcohol, e.g., cetyl alcohol, is assumed to influence the rigidity of the oil/water interface or lower the interfacial tension. However, Table 2 shows a small discrepancy between costabilized and noncostabilized oil/polymer interfacial values. The reason for this is that the contact angles are calculated by eq 1. A small error in the observation of the force value (F) (as obtained from force/immersion curves) will result in a large deviation when calculating the contact angle θ, hence producing variations between contact angles for costabilized and noncostabilized systems. However, when the interfacial tension values are calculated by eq 2, the discrepancy in contact angle values are again reduced, thus leading to small differ-

Table 2. Results Showing the Interfacial Tension (γ_{ij}) and Spreading Coefficient (S_i) Data and Subsequent Predicted Morphologies[a]

PBA oil	costabilizer	θ_{op}	θ_{pw}	γ_{op}	γ_{pw}	γ_{ow}	S_1	S_2	S_3	morphology prediction
D		12.5	73.4	9.3	23.2	7	<0	<0	>0	core/shell
D	HD	8.9	73.4	8.8	23.2	6.9	<0	<0	>0	core/shell
HD		48.1	73.4	14.6	23.2	6.7	<0	<0	>0	core/shell
SO		28.3	73.4	13.9	23.2	9.7	<0	<0	<0	acorn
SO	HD	29.6	73.4	14.1	23.2	9.7	<0	<0	<0	acorn
OO		60.8	73.4	16.8	23.2	1.7	<0	<0	>0	core/shell
OO	HD	57.8	73.4	15.3	23.2	1.7	<0	<0	>0	core/shell
PO		59	73.4	17.4	23.2	9.1	<0	<0	<0	acorn
PO	HD	54.3	73.4	15.3	23.2	9.2	<0	<0	<0	acorn
O		36.2	73.4	10.1	23.2	1.1	<0	<0	>0	core/shell
O	HD	35.9	73.4	10.1	23.2	1.1	<0	<0	>0	core/shell

[a] θ_{op} and θ_{pw} denote the contact angle between the oil/polymer and polymer/water, respectively. γ_{ij} represents the interfacial tension value corresponding to the oil/polymer (op), polymer/water (pw), and oil/water (ow) phase (D = decane, HD = hexadecane, SO = silicone oil, OO = olive oil, PO = paraffin oil, O = 1-octanol).

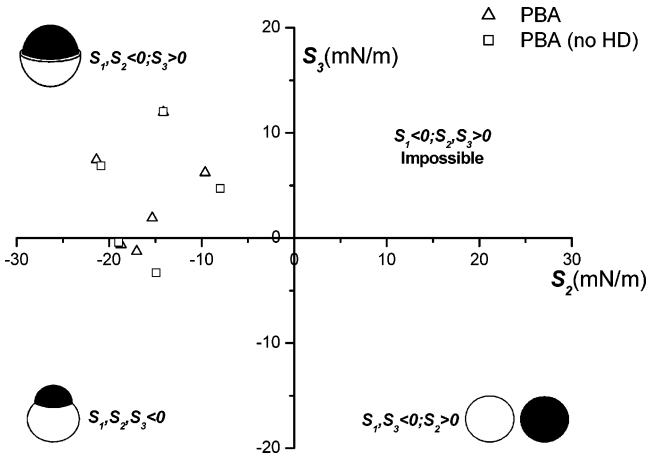

Figure 3. Graphical representation of spreading coefficients (S_i) and predicted morphologies.

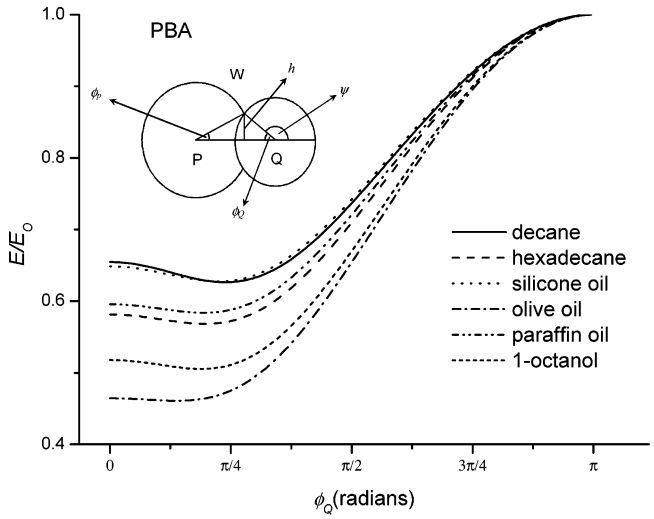

Figure 4. Traces showing the change in energy as a function of ϕ_Q (degree of engulfment) for the engulfment of different oils by PBA.

ences between interfacial tension values, thereby not influencing spreading coefficients.

In other words, the addition of hexadecane will in no way influence the interfacial tensions and, therefore, the outcome of spreading coefficients.

Figure 3 shows the spreading coefficient values and consequent predicted morphologies for the different PBA/oil systems.

Although the predictions according to the spreading coefficients return values such as core/shell or acorn, care must be taken with the interpretation of these results. For the spreading predictions to be valid it was taken that $\gamma_{12} > \gamma_{23}$. Phase 12 corresponds to the polymer/water interface and phase 23 to the oil/water interface, hence showing that the interfacial tension between the oil and water is lower than the interfacial tension between the polymer and water. Thermodynamically, the driving force will therefore be to form an oil layer between the water and polymer phases because of the drive to lower energies. This becomes clearer when looking at predictions done according to the work of Waters.[32,33] In this instance the engulfing polymer is chosen, and the energy is monitored as a function of engulfment. Predictions were performed by substituting the interfacial tension values into

$$E = (\pi/2)^{1/3}(3v_Q)^{2/3}[\gamma_{P-W}(1 + \cos\phi_p)\sin^2\phi_Q/\sin^2\phi_p + \gamma_{Q-W}(1 + \cos\phi_Q) + \gamma_{P-Q}(1 - \cos\phi_Q)] \quad (4)$$

where γ_{ij} is the interfacial tensions between the P−Wth, Q−Wth, and P−Qth interface (see Figure 4), v_Q is the volume fraction of the core polymer, ϕ_Q is known ($0 \leq \phi_Q \leq \pi$), and ϕ_p is determined through a reiteration process. Plots of E/E_0 vs ϕ_Q where

$$E_0 = 2(\pi/2)^{1/3}3^{2/3}[\gamma_{P-W} + v_Q^{2/3}\gamma_{P-Q}] \quad (5)$$

will indicate whether an intermediate morphology has a lower interfacial energy than the engulfed structure and the degree of engulfment which corresponds to the lowest energy.

Energy traces for the PBA−oil systems are shown in Figure 4. From this it follows that the energy increases if the oil is used as the engulfed (Qth) phase and the polymer as the engulfing (Pth) phase, hence evidently indicating an inverted core/shell morphology. These results suggest that the predictions from Torza/Mason and from Waters both point to an inverted core/shell morphology. Nevertheless, an experimental verification of the PBA/HD system was worthwhile.

Evaluation of a PBA/HD Latex System. To check the validity of the predictions, a PBA/HD latex was synthesized and analyzed. For initial experiments the PBA was lightly cross-linked, and no grafting was performed. Film formation was evaluated after casting of the latex on a silica substrate. AFM images in Figures 5a−f show clearly the effect of film formation at room temperature. Non-cross-linked PBA has a T_g of −55 °C, and even a lightly cross-linked PBA will show immedi-

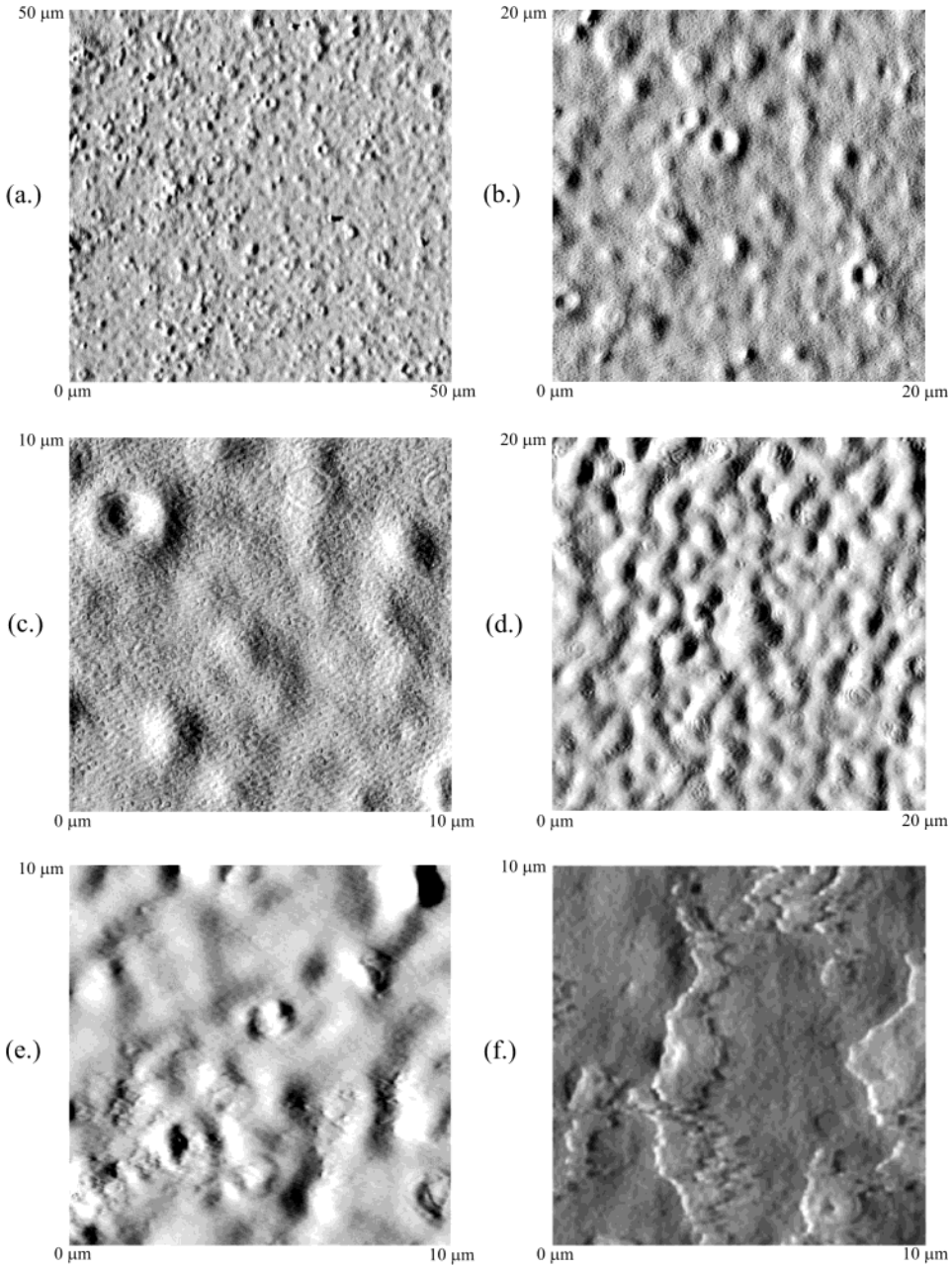

Figure 5. AFM images showing the film formation of PBA/HD core/shell particles at room temperature. (a)−(c) show different magnifications of the same sample area whereas (b) and (d)−(f), consecutively, show film formation of the same sample area as a function of time.

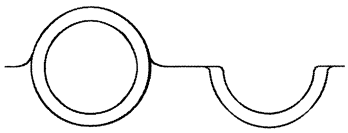

Figure 6. Interpretation of "bumps" and "potholes" as seen during AFM analysis of the film formation of PBA/HD core/shell particles.

ate spreading at room temperature. In Figure 5b the presence of "bumps" and "potholes" can be seen. The bumps represent intact particles while the potholes are representative of collapsed particles, which point to the initial formation of core/shell particles (cavities) (Figure 6). At the end of the film formation no more cavities are left, and a smooth surface can be distinguished in Figure 5f. Initial AFM experiments therefore show discrepancies to predictions made, and these discrepancies are backed by additional TEM analyses.

For TEM analyses the initial PBA shell was strengthened by cross-linking as well as grafting of methyl methacrylate (MMA) onto the primary PBA shell. Strengthening of the particles had to be done for TEM sample preparation. The lack of stability would lead to a destroyed morphology during embedding and curing of the particles in the epoxy resin as well as physical deformation and extraction of the particles when cut with a diamond knife during the ultramicrotoming process.

Figure 7a−d shows TEM images of the particles, clearly indicating core/shell formation. The stained areas are representative of the poly(meth)acrylates while the lighter areas represent the core oil. It is clear that the morphology predicted does not correspond to

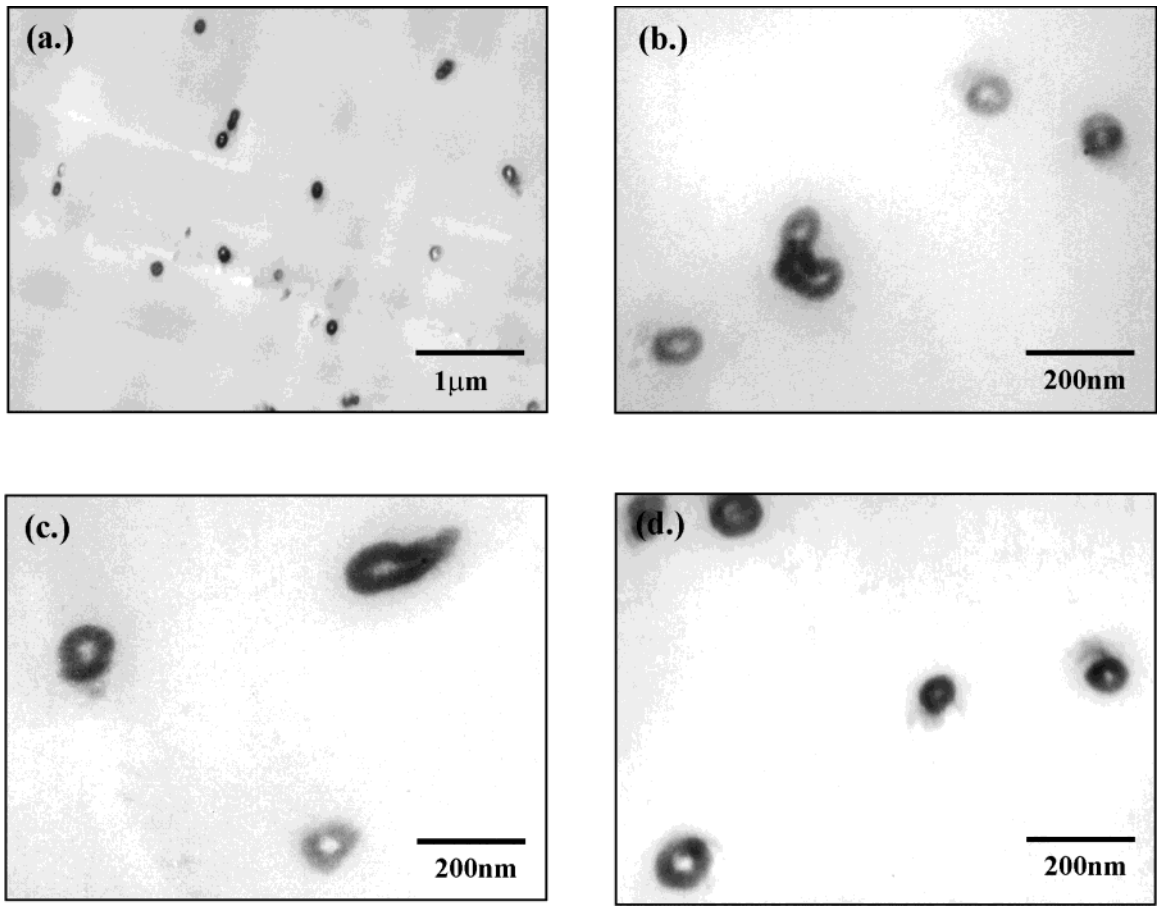

Figure 7. TEM images of the synthesized PBA/HD core/shell particles: (a) a low-magnification TEM of the synthesized particles; (b)−(d) high-magnification images of different sections on the microtomed sample.

the morphology that was obtained experimentally. Clearly, other effects contribute to the formation of proper core/shell particles, and these effects must overrule the thermodynamic effects.

Thermodynamic vs Kinetic Control of Particle Morphology. Particle morphology can be controlled by two factors, namely thermodynamics and kinetics. Unfortunately, the assumption is usually made that the equilibrium morphology of the final latex composite particle is determined by the thermodynamic part of the equation while the kinetic part will only determine the ease with which the thermodynamically favored morphology can be achieved. As an example, the work of Torza and Mason can be mentioned where the thermodynamics of the system were the key factor in controlling the equilibrium morphology due to the high mobility of the liquid phases.[17] However, in 1985 Cho et al.[35] discussed the anchoring effect of ionic terminal groups that are introduced into the sample through the use of an ionic initiator. Other factors that were investigated in their work included swelling time, pH, and viscosity at the polymerization loci. This was done to explain the change in particle morphology that takes place during a polymerization reaction. The difference in hydrophobicity of the constituting phases should have an influence on the outcome of the particle morphology. However, Cho et al. found that this was not the case but that morphological changes could rather be related to the type and concentration of initiator used and to the polymerization temperature. In the case of potassium persulfate (KPS) the initiator will fragment into two identical primary radicals, which will initiate polymerization. However, on entering the droplet the terminal $-SO_4^-$ end group will anchor itself at the water/oil interface, leading to an anchoring effect and thereby influencing morphology. A graphical representation is shown in Figure 8. Because of the surfactant-like nature of the oligomeric radical (polar headgroup, nonpolar tail), the anchoring effect will also play an important role in the reduction of the interfacial tension and in increasing the surface polarity of the latex particles.

The rate of morphological change from one situation to the other is dependent on the diffusional resistance (which is related to chain mobility). A low viscosity at the polymerization locus will enhance the mobility of the polymer chains. This will enhance the migration of the two immiscible phases into two different domains, thus being able to adopt thermodynamically favored morphologies. A high local viscosity, on the other hand, will create a kinetic barrier toward polymer chain diffusion and decrease the degree of phase separation. The competition between phase separation and polymerization kinetics will be the determining factor in the generation of nonequilibrium morphologies. Cho et al. summarized their findings, and this summary can be seen in Figure 9.[35]

Further evidence of kinetically controlled particle morphology was given in 1990 by Mills et al.,[36] who considered the dependence of the morphology on various factors including rate of diffusion, propagation, termination, entry, transfer, and exit. To do this, the monomer and free-radical concentrations in particles were calculated as a function of position and time using "pseudo-bulk" equations.[37] These equations were extended[36] to

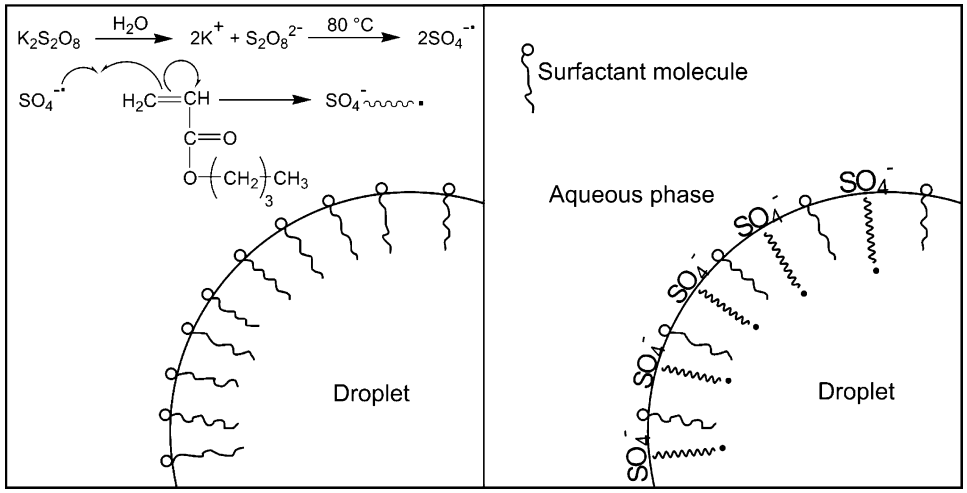

Figure 8. Anchoring effect caused by the interaction between entering radicals and surfactant.

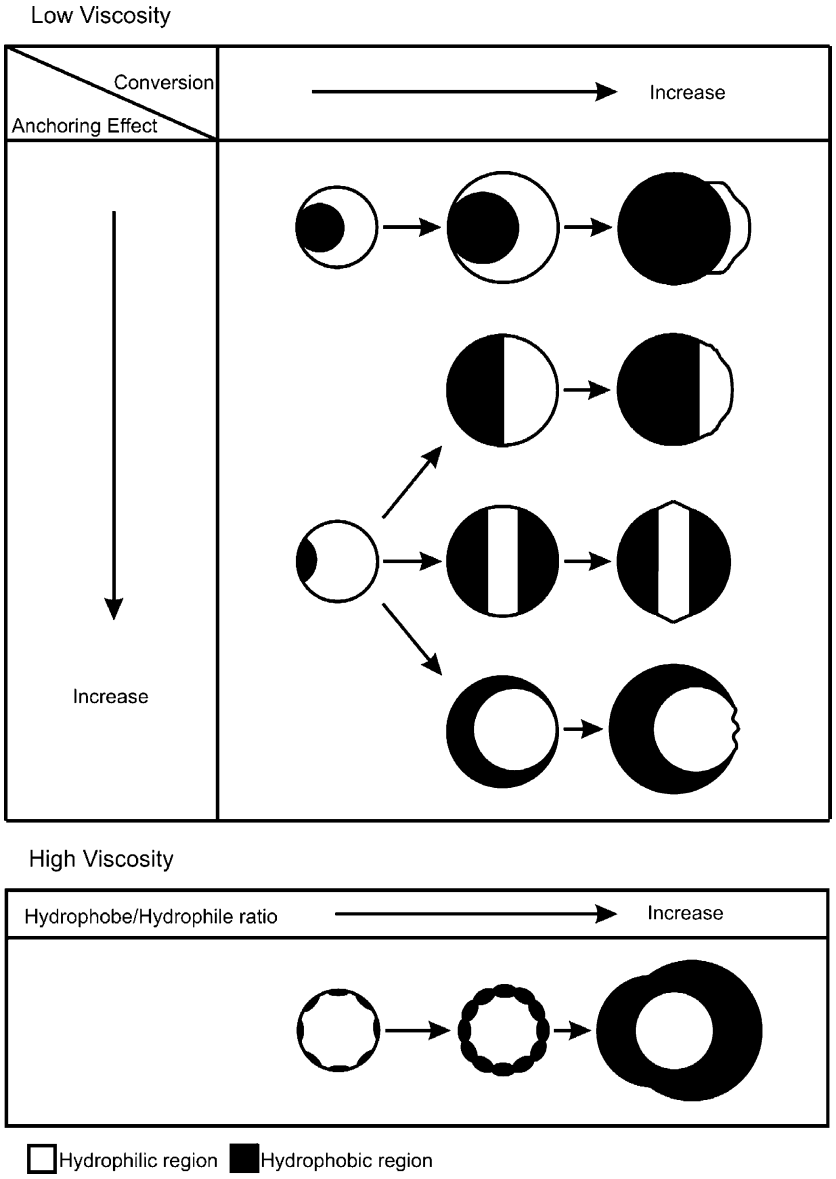

Figure 9. Influence of the degree of anchoring, conversion, and viscosity on the outcome of particle morphology.[35]

take into account diffusion, spatial inhomogeneities, and the chain length dependent termination kinetics. Instead of only using single free-radical species $R(r,t)$ (which is the concentration of free radicals as a function of time and position in a particle), long radicals and relatively mobile short radicals were considered. Entering radicals can be seen as long due to the surface anchoring effect of the hydrophilic end group while

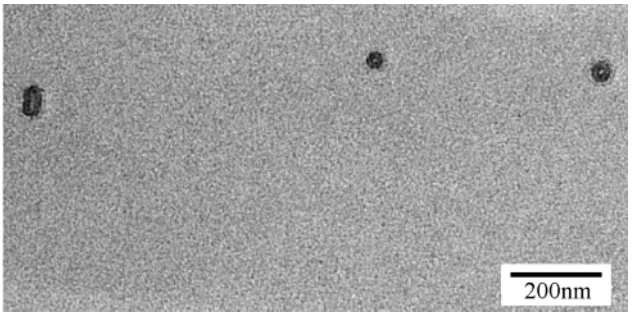

Figure 10. TEM image of core/shell particles synthesized with the use of a redox initiator.

exiting radicals must be short to be reasonably soluble in the aqueous phase. A number of very important deductions were made from these kinetic studies, e.g., (1) the probability to produce a core/shell morphology will increase when the rate coefficient of entry of free radicals is sufficiently high (e.g., in the case of a redox initiator), and (2) a higher tendency for core/shell morphology is possible when the rate of termination is high relative to the rate of diffusion.

The deviation from thermodynamically controlled particle morphology has been mentioned by many other authors including Jönsson et al.[38] and Muscato et al.[39]

A further study into the effect of chain mobility on the obtained morphology was undertaken by changing the initiation system. Two aspects of the initiation system were taken into consideration: first, the anchoring effect, which is present in the case of a charged primary radical (viz. KPS), and, second, the locus of generation of primary radicals. In this study the initiator was changed to AIBN as well as to a redox initiator.

For the redox initiator, cumyl hydroperoxide with Fe^{2+} was chosen. This system is the same as was used for the grafting of the MMA onto the initial PBA shell. CHP is oil-soluble and will enter the droplets when added to the miniemulsified system. However, CHP only dissociates with an appreciable rate in conjunction with the transition metal complex (Fe^{2+}/EDTA), which is water-soluble. Therefore, the primary radical producing reaction can only take place at the oil/water interface. Results of the experiment with redox initiation can be seen in Figure 10.

AIBN was used as an oil-soluble initiator that will generate primary radicals throughout the organic phase. AIBN has no ionic group that can establish surface anchoring and shows slightly higher rates of dissociation compared to that of KPS.[40] Thus, although AIBN has a degree of water phase initiation,[41,42] the entering radicals will not be able to anchor themselves at the water/droplet interface, and primary radicals will also be created in the interior of the latex particle. The result of the AIBN-initiated polymerization can be seen in Figure 11.

The main difference between the AIBN-initiated system and the KPS or CHP/Fe^{2+}-initiated systems is the solid particles obtained in the former and the core/shell particles obtained in the latter case. KPS leads to surface anchoring as discussed above. However, both CHP and AIBN yield oil-soluble primary radicals that do not seem to have a particular preference for the oil−water interface. As mentioned, AIBN and CHP/Fe^{2+} differ in their locus of primary radical generation. The essential question then is, how fast is initiation/propagation compared to diffusion? More precisely, is a primary radical or short chain oligomer able to diffuse throughout the particle before it has grown to a chain length that virtually immobilizes it? An accurate assessment of diffusivity vs polymerization kinetics is quite complicated. Therefore, we limit the assessment to an order of magnitude estimation of the so-called Damköhler number (*Da*).[43] This is a dimensionless number that indicates whether a reaction is diffusion-controlled or chemically controlled. The Damköhler number is defined as follows:

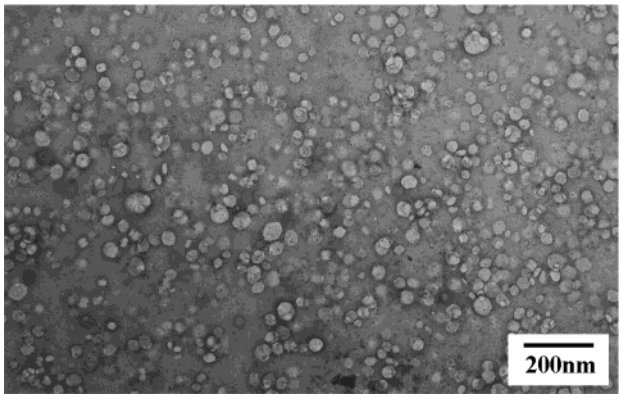

Figure 11. TEM image of solid particles synthesized with the use of an oil-soluble initiator (AIBN).

$$Da = \frac{k_p[M]}{D/d^2} \tag{6}$$

where D is the diffusion coefficient of a low molar mass species in a semidilute polymer solution, k_p is the propagation rate constant of a growing radical (or initiation rate constant of a primary radical), [M] is the monomer concentration at the locus of polymerization, and d is the relevant diffusion distance. Typical values for these quantities are $D = 10^{-9}$ m^2 s^{-1}, $k_p = 10^4$ L mol^{-1} s^{-1}, [M] = 5 mol L^{-1}, and $d = 10^{-8}$ m. This would result in $Da = 5 \times 10^{-3}$, which is indicative of a system without transport limitation ($Da \ll 1$). Nevertheless, core/shell morphology is observed in the CHP/Fe^{2+}-initiated system. One of the likely origins of the difference in morphology between AIBN and CHP/Fe^{2+} is hydrogen abstraction from already formed PBA. The cumyloxy radical has a relatively strong tendency toward H abstraction,[44] and the cumyloxy radicals are formed at the oil−water interface. This may lead to branched or even cross-linked polymer in the outer shell of the particle. This in turn will limit the mobility of the polymer and lead to core/shell morphology.

From the results it is thus quite clear that core/shell morphology can be obtained when radicals are formed at the oil/water interface and if diffusion to the interior of the particle is restricted.

Conclusions

Core/shell particles with liquid cores were synthesized by an in situ miniemulsion polymerization process. Morphology predictions were performed on the investigated system, and it was found that predicted and observed morphologies did not coincide. The reason for this discrepancy is that current prediction models are only based on thermodynamic considerations and not kinetic considerations. Deviation from the predicted morphology can be caused by the type and amount of surfactant and type of initiator used. Selection of the

proper initiator type can lead to anchoring of entering radicals. This will reduce the ability of radicals to diffuse to the inside of the droplet. Polymerization will therefore occur preferentially at the oil/water interface, thereby causing a phase separation between the polymer and core oil and thus forming the desired core/shell particles with liquid cores. This reasoning was further strengthened by changing the type of initiator. AIBN provides no surface anchoring. In this instance the thermodynamically preferred morphology, which is inverse core/shell, will dominate, thus causing solid poly(butyl acrylate) particles. The redox initiator (CHP/Fe^{2+}) was used to specifically create primary radicals at the water/oil interface. The fact that this way of initiation leads to core/shell particles is most likely due to significant branching, which leads to decreased mobility of the chains throughout the particle.

Acknowledgment. The authors thank Drs. M. Jaffer (University of Cape Town) and J. Loos (Technical University of Eindhoven) for TEM imaging. Prof. B. Vincent (University of Bristol) is gratefully acknowledged for stimulating discussions. The project was funded by the Dutch Polymer Institute (DPI), and further financial support was provided by the National Research Foundation of South Africa (NRF).

References and Notes

(1) Caruso, F. In *Nano-Surface Chemistry*; Rosoff, M., Ed.; Marcel Dekker: New York, 2002; pp 505−525.
(2) Dimonie, V. L.; Daniels, E. S.; Shaffer, O. L.; El-Aasser, M. S. In *Emulsion Polymerization and Emulsion Polymers*; Lovell, P. A., El-Aasser, M. S., Eds.; John Wiley & Sons Ltd.: Chichester, 1997; pp 293−326.
(3) Strauss, J. *Surf. Coat. Aust.* **1987**, *24*, 6−15.
(4) Davis, S. S.; Illum, L. *Biomaterials* **1988**, *9*, 111−115.
(5) Romero-Cano, M. S.; Vincent, B. *J. Controlled Release* **2002**, *82*, 127−135.
(6) Grancio, M. R.; Williams, D. J. *J. Polym. Sci., Part A-1* **1970**, *8*, 2617−2629.
(7) Arshady, R. *Polym. Eng. Sci.* **1989**, *29*, 1746−1758.
(8) Arshady, R. *Polym. Eng. Sci.* **1990**, *30*, 905−914.
(9) Frère, Y.; Danicher, L.; Gramain, P. *Eur. Polym. J.* **1998**, *34*, 193−199.
(10) Arshady, R. *Polym. Eng. Sci.* **1990**, *30*, 915−924.
(11) Jung, M. *Polymerization in Bilayers*; Technische Universiteit Eindhoven: Eindhoven, 2000.
(12) Sudol, E. D.; El-Aasser, M. S. In *Emulsion Polymerization and Emulsion Polymers*; Lovell, P. A., El-Aasser, M. S., Eds.; John Wiley and Sons Ltd.: England, 1997; pp 699−722.
(13) Schellenberg, C.; Akari, S.; Regenbrecht, M.; Tauer, K.; Petrat, F. M.; Antonietti, M. *Langmuir* **1999**, *15*, 1283−1290.
(14) Landfester, K.; Boeffel, C.; Lambla, M.; Spiess, H. W. *Macromolecules* **1996**, *29*, 5972−5980.
(15) Dobashi, T.; Yeh, F.-J.; Ying, Q.; Ichikawa, K.; Chu, B. *Langmuir* **1995**, *11*, 4278−4282.
(16) Sekine, K.; Hanai, T. *Colloid Polym. Sci.* **1991**, *269*, 880−888.
(17) Torza, S.; Mason, S. G. *J. Colloid Interface Sci.* **1970**, *33*, 67−83.
(18) Loxley, A.; Vincent, B. *J. Colloid Interface Sci.* **1998**, *208*, 49−62.
(19) Lee, S.; Rudin, A. In *Polymer Latexes: Preparation, Characterization and Applications*; Daniels, E. S., Ed.; American Chemical Society: Washington, DC, 1992; pp 234−254.
(20) Winzor, C. L.; Sundberg, D. C. *Polymer* **1992**, *33*, 3797−3810.
(21) Sundberg, D. C.; Casassa, A. P.; Pantazopoulos, J.; Muscato, M. R.; Kronberg, B.; Berg, J. *J. Appl. Polym. Sci.* **1990**, *41*, 1425−1442.
(22) Sundberg, E. J.; Sundberg, D. C. *J. Appl. Polym. Sci.* **1993**, *47*, 1277−1294.
(23) Stubbs, J. M.; Sundberg, D. C. *J. Coat. Technol.* **2003**, *75*, 59−67.
(24) Wang, C. C.; Yu, N. S.; Chen, C. Y.; Kuo, J. F. *J. Appl. Polym. Sci.* **1996**, *60*, 493−501.
(25) Wang, C. C.; Yu, N. S.; Chen, C. Y.; Kuo, J. F. *Polymer* **1996**, *37*, 2509−2516.
(26) Domingue, J. *Am. Lab.* **1990**, 50−55.
(27) Wu, S. *Polymer Interface and Adhesion*; Marcel Dekker Inc.: New York, 1982.
(28) Van Krevelen, D. W. *Properties of Polymers. Their Correlation with Chemical Structure; their Numerical Estimation and Prediction from Additive Group Contributions*; Elsevier Science B. V.: Dordrecht, The Netherlands, 1997.
(29) Lide, D. L. *CRC Handbook of Chemistry and Physics*, 76th ed.; CRC Press Inc.: Boca Raton, FL, 1995.
(30) Wu, S. *J. Macromol. Sci., Rev. Macromol. Chem.* **1974**, *C10*, 1−73.
(31) Sue, H. J.; Garcia-Meitin, E. I.; Burton, B. L.; Garrison, C. C. *J. Polym. Sci., Part B: Polym. Phys.* **1991**, *29*, 1623−1631.
(32) Waters, J. A. *Colloids Surf., A* **1994**, *83*, 167−174.
(33) Waters, J. A. In *Colloidal Polymer Particles*, 2nd ed.; Goodwin, J. W., Buscall, R., Eds.; Academic Press Limited: London, 1995; pp 113−135.
(34) Landfester, K.; Bechtold, N.; Tiarks, F.; Antonietti, M. *Macromolecules* **1999**, *32*, 5222−5228.
(35) Cho, I.; Lee, K.-W. *J. Appl. Polym. Sci.* **1985**, *30*, 1903−1926.
(36) Mills, M. F.; Gilbert, R. G.; Napper, D. H. *Macromolecules* **1990**, *23*, 4247−4257.
(37) Ballard, M. J.; Napper, D. H.; Gilbert, R. G. *J. Polym. Sci., Polym. Chem. Ed.* **1984**, *22*, 3225−3253.
(38) Jönsson, J.-E.; Hassander, H.; Törnell, B. *Macromolecules* **1994**, *27*, 1932−1937.
(39) Muscato, M. R.; Sundberg, D. C. *J. Polym. Sci., Part B: Polym. Phys.* **1991**, *29*, 1021−1024.
(40) *Polymer Handbook*, 2nd ed.; Wiley-Interscience: New York, 1975.
(41) Luo, Y.; Schork, F. J. *J. Polym. Sci., Part A: Polym. Chem.* **2002**, *40*, 3200−3211.
(42) Blythe, P. J.; Klein, A.; Phillips, J. A.; Sudol, E. D.; El-Aasser, M. S. *J. Polym. Sci., Part A: Polym. Chem.* **1999**, *37*, 4449−4457.
(43) Thoenes, D. *Chemical Reactor Development from Laboratory Synthesis to Industrial Production*; Kluwer Academic Publishers: Dordrecht, 1994.
(44) Moad, G.; Solomon, D. H. *The Chemistry of Free Radical Polymerization*; Pergamon Press: Oxford, 1995.

MA034596X